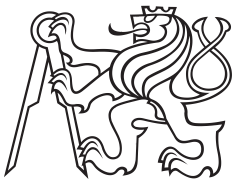

Czech Technical University in Prague

F4

Faculty of Nuclear Sciences and Physical Engineering

Mathematical modeling and numerical simulations of turbulent flows

Doc. Ing. Jiří Fürst, PhD.

2020

Summary

The lecture deals with the development of mathematical models describing turbulent flows of compressible fluids and their approximation by finite volume method. The basis of mathematical models are the time-averaged Navier-Stokes equations equipped with an additional turbulence turbulence model. a model for transition from laminar to turbulent mode. One specific transition and turbulence model from the literature is briefly described along with its improvements proposed by the author of the lecture. The next section describes the approximation of models using the finite volume method. The approximation of convective terms using the WLSQR method proposed by the author is described more in details. Next, the construction of a matrix-free implicit symmetric Gauss-Seidel method is described. Two examples of application of described models and methods are given in the final part of the lecture. The first example shows that it is necessary to pay attention both to the choice of mathematical model and its numerical model approximation. The second case shows a real application of described models and methods for analysis of the radial turbine of a turbocharger.

Keywords: Compressible flows; Finite volume method; High order method; Implicit method; Turbulence model; Laminar-turbulent transition

Souhrn

Přednáška se zabývá vývojem matematických modelů popisujících turbulentní proudění stlačitelné tekutiny a jejich aproximací metodou konečných objemů. Základem matematických modelů jsou přitom časově středované Navierovy-Stokesovy rovnice doplněné o vhodný model turbulence případně o model zachycující přechod z laminárního to turbulentního režimu. V přednášce je stručně popsán jeden z modelů dostupný v literatuře spolu s jeho vylepšením navrženým autorem přednášky. V další části je popsána aproximace modelů pomocí metody konečných objemů. Podrobněji je rozebrána aproximace konvektivních členů pomocí autorem navržené WLSQR metody a konstrukce implicitní metody založené na symetrické Gaussově-Seidelově metodě. V závěrečné části jsou uvedeny dva příklady aplikace popisovaných modelů a metod. První z příkladů ukazuje, že je při simulacích turbulentního proudění nutné věnovat pozornost jak volbě matematického modelu, tak jeho numerické aproximaci. Druhý případ ukazuje reálnou aplikaci modelů a metod pro analýzu radiální turbíny turbodmychadla.

Klíčová slova: Stlačitelné proudění; metoda konečných objemů; metoda vysokého řádu; implicitní metoda; model turbulence; přechod do turbulence

Překlad názvu: Matematické modelování a numerické simulace turbulentního proudění

Contents

Chapter 1

Introduction

The turbulence represents a very difficult and complex problem both for mathematics as well as for classical physics. Despite the fact that the earliest description of turbulence due to da Vinci is more than 500 years old, the exact definition of turbulence is still not known. The da Vinci's description of the turbulent motion *"...the smallest eddies are almost numberless, and large things are rotated only by large eddies and not by small ones, and small things are turned by small eddies and large"* is surprisingly modern and describes well one of the features of turbulent motion: the broadband spectrum of turbulence with energy cascade. Since then, many attempts to define formally the turbulence have appeared. Let us mention for example the definition by T. von Kármán [1]: *"Turbulence is an irregular motion which in general makes its appearance in fluids, gaseous or liquid, when they flow past solid surfaces or even when neighboring streams of the same fluid flow past or over one another."* or a more modern definition by Hinze [2]: *"Turbulent fluid motion is an irregular condition of the flow in which the various quantities show a random variation with time and space coordinates, so that statistically distinct average values can be discerned."* Very useful definition of turbulence has been given by Chapman and Tobak [3]: *"Turbulence is any chaotic solution to the 3-D Navier-Stokes equations that is sensitive to initial data and which occurs as a result of successive instabilities of laminar flows as a bifurcation parameter is increased through a succession of values."* Although the last definition is far from being an ultimate answer to the problem of turbulence, it contains many important observations:

- the turbulent motion of the fluid is described by the set of **Navier-Stokes equations**,
- as such, the turbulent motion is **deterministic** although it has **chaotic** behavior,
- turbulent motion (or turbulence) occurs at high Reynolds number.

Taking into account other definition, one can point out also another properties of the turbulence:

- **irregularity** - although the turbulence is deterministic, the motion is chaotic, seemingly random,

- **diffusivity** - the turbulence enhances mass, heat, and momentum transfer,
- **3D character** - turbulent flows have three-dimensional nature with fluctuating vorticity,
- **dissipation** - turbulent flows are always dissipative with the energy of large scale structures being transferred to small structured mostly by inviscid effect (vortex breakup) and the dissipated,
- **broadband spectrum** - the turbulent flow contains an extremely large range of length and time scales.

There are many directions of research concerning the turbulence including among others mathematical theory of dynamic systems, new physical theories concerning e.g. the transition from laminar to turbulent flows, or new experimental methods. This lecture is devoted especially to the mathematical modeling of turbulence flows with technical applications. Using all the above mentioned definitions, one can conclude that an appropriate mathematical model should be based on the Navier-Stokes equations[1] (either for compressible or incompressible fluids). Moreover, from the engineering point of view, the model should be able to predict statistical quantities (e.g. time averaged lift of the wing) with reasonable computational effort.

The state of the art methods date back to 1970 when Deardorff [6] proposed a large eddy simulation (**LES**) where the effect of largest eddies are resolved whereas smaller eddies are modeled with a so called sub-grid model. The first direct numerical simulation (**DNS**) was achieved by Orzsag and Paterson in 1972, see [7]. The DNS method solves the Navier-Stokes equations for whole spectrum of length scales and therefore does not need any additional model. Unfortunately, both the DNS and LES method are not feasible for practical computations due to extremely large computational costs. The spatial requirements for DNS are of the order of $Re_T^{9/4}$ where $Re_T = u'l/\nu$ is the turbulent Reynolds number related to the magnitude of velocity fluctuations of the largest vortices u' and its size l. The total computing costs is then of the order of Re_T^3, see e.g. [8]. Although the LES method promises slightly lower computational costs, its applications for wall bounded flows is almost as expensive as the DNS. On the other hand, the Reynolds averaged Navier-Stokes approach (**RANS**) proposed e.g. by Launder and Spalding in [9] provided a viable alternative. The RANS approach assumes an averaged system of Navier-Stokes equations for time (or ensemble) averaged quantities with an additional model for the so called Reynolds stress tensor $\tau_{ij} = - < u_i' u_j' >$.

There are many additional turbulence models with different levels of complexity starting from a very simple algebraic models (see e.g. [10]), through

[1] Although th Navier-Stokes equations represent a building block for mainstream turbulence modeling research, there are also other promising approaches including the lattice-Boltzmann method [4], or smoothed particle hydrodynamics [5].

more advanced one- or two-equations models (see e.g. [9], [11], [12], [13]) to the computationally expensive full Reynolds stress models [14].

Although the RANS approach represents a workhorse for many technical applications, there are known limitations of the modeling approach. The usability of the modeling can be extended using a hybrid method combining the LES approach far from solid walls with RANS approach in boundary layers, see e.g. detached eddy simulation (**DES**) [15], or partially averaged Navier-Stokes method (**PANS**) [16]. These methods becomes feasible thanks to massive progress in computer power during last years. However the trend is moving from RANS to LES (or rather hybrid RANS-LES) models, the importance of RANS approach remains in the solution in near wall region.

The lecture will cover two main topics connected with the applications of turbulence modeling in engineering. The first one deals with the development of advanced transition and turbulence models compatible with RANS approach. The second topic focuses on the numerical solution of Navier-Stokes or RANS equations especially for the case of high speed flows of compressible fluids. The last section shows some applications of mentioned advanced turbulence models and numerical methods in engineering.

Chapter 2

Advanced turbulence models

The first part of the lecture is devoted to the development of a turbulence model. We limit ourself to standard RANS approach based on the eddy viscosity here. Although the eddy viscosity approach has many known weaknesses, it still represents the mainstream method in turbulence modeling for engineering purposes due to relatively low computational cost. During almost 50 years a large number of turbulence models was proposed. Let us mention e.g. the well known two equation $k-\epsilon$ model [9], one-equation Spalart-Allmaras model [17], or the two-equation $k-\omega$ SST model [12]. Over the course of years, a number of modifications or new models improving the predictive capabilities in specific cases have arisen. To date, however, a universal model has not been developed to capture all aspects of turbulent flows.

The motion of a compressible fluid is described by the set of Navier-Stokes equations

$$\frac{\partial \rho}{\partial t} + \nabla \cdot (\rho \vec{u}) = 0, \tag{2.1}$$

$$\frac{\partial (\rho \vec{u})}{\partial t} + \nabla \cdot (\rho \vec{u} \otimes \vec{u}) + \nabla p = \nabla \cdot \vec{\vec{\tau}}, \tag{2.2}$$

$$\frac{\partial (\rho E)}{\partial t} + \nabla \cdot (\rho H \vec{u}) = \nabla \cdot (\vec{\vec{\tau}} \cdot \vec{u}) - \nabla \cdot \vec{q}, \tag{2.3}$$

where ρ is the density, $\vec{u}$ is the velocity, p is the pressure, $E = e + (\vec{u} \cdot \vec{u}/2)$ is the total specific energy, $H = E + p/\rho$ is the total specific enthalpy, $\vec{\vec{\tau}}$ is the viscous stress tensor, and $\vec{q}$ is the heat flux. The system is closed by additional constitutive laws including the equation of state, Fourier's law, or Stokes law. The system can be rewritten in simple vectorial form

$$\frac{\partial \mathbf{W}}{\partial t} + \nabla \cdot \vec{\mathbf{F}}^c(\mathbf{W}) = \nabla \cdot \vec{\mathbf{F}}^v(\mathbf{W}, \nabla \mathbf{W}), \tag{2.4}$$

where $\mathbf{W}$ is the vector of conservative variables $[\rho, \rho\vec{u}, \rho E]^T$, $\vec{\mathbf{F}}^c$ are the convective fluxes (see the left hand side of (2.1)-(2.3)), and $\vec{\mathbf{F}}^v$ are the viscous fluxes (the right hand side of (2.1)-(2.3)).

Although the system (2.4) describes both laminar and turbulent flow regimes, the direct simulation (DNS) is too expensive for engineering needs.

Therefore one deals either with Reynolds (or Favre) averaged (RANS) or filtered (LES) equations. In both cases, the RANS or LES equations can be written in similar form as the equation (2.4) for averaged (or filtered) quantities with $\vec{\vec{\tau}}$ and $\vec{q}$ replaced by the effective stress tensor and effective heat flux and with some additional convection-diffusion equations for turbulence model. As an example, let's mention the two-equation $k-\omega$ SST model originally proposed in [12]. The model assumes two additional equations for turbulent kinetic energy $k =< u_i' u_i' > /2$ and specific dissipation rate ω (see [12] for details)

$$\frac{\partial(\rho k)}{\partial t} + \nabla \cdot (\rho k \vec{u}) = P_k - \beta^* \rho k \omega + \nabla \cdot [(\mu + \sigma_k \mu_t) \nabla k] \,, \tag{2.5}$$

$$\frac{\partial(\rho \omega)}{\partial t} + \nabla \cdot (\rho \omega \vec{u}) = P_\omega - \beta \rho \omega^2 + \nabla \cdot [(\mu + \sigma_\omega \mu_t) \nabla \omega] + C D_\omega. \tag{2.6}$$

The turbulent viscosity $\mu_t = \rho a_1 k / \max(a_1 \omega, \Omega F_2)$ is then used for modeling the effective stress tensor

$$\vec{\vec{\tau}} = 2(\mu + \mu_t)\vec{\vec{S}} - \frac{2}{3}\rho k \vec{\vec{\mathbb{I}}}, \tag{2.7}$$

where $\vec{\vec{S}} = [\nabla \vec{u} + (\nabla \vec{u})^T]/2 - (\nabla \cdot \vec{u})\vec{\vec{\mathbb{I}}}/3$ is the trace-less strain rate tensor and μ is the viscosity of the fluid.

2.1 Transition and turbulence model

Turbulence models are in general developed and calibrated for fully turbulent flows. In the reality, however, the structure of boundary layers is much more complicated. The flow is in the vicinity of the leading edge of a profile usually laminar and the turbulence arises later downstream when the Reynolds number related to stream-wise position reaches certain value - the so called critical Reynolds number. Unfortunately the value of the critical Reynolds number is not universal and vary by several orders of magnitude. For an accurate prediction of flow field a special transition model has to be used. During last few years, several transition and turbulence models have been proposed in the literature. Let's mention the e^N model [18], the algebraic intermittency model [19], the four-equation transition and turbulence model [20], or the three-equation $k - k_L - \omega$ model [21].

Let's focus the attention to latter model proposed in [21]. The model assumes additional three equations for the turbulent kinetic energy k_T, for the so called laminar kinetic energy k_L, and for the specific dissipation rate ω. The meaning of k_T and ω is the same as k and ω in the standard $k-\omega$ turbulence model. The laminar kinetic energy k_L expresses laminar fluctuations in the pre-transitional region (e.g. the so called Tollmien-Schlichting waves). The model equations for compressible flows are given bellow [21]

$$\frac{\partial(\rho k_T)}{\partial t} + \nabla\cdot(\rho k_T \vec{u}) = \rho(P_{k_T} + R_{BP} + R_{NAT} - k_T\omega - D_T) + \\ +\nabla\cdot\left[\left(\mu + \frac{\rho\alpha_T}{\sigma_k}\right)\nabla k_T\right], \tag{2.8}$$

$$\frac{\partial(\rho k_L)}{\partial t} + \nabla\cdot(\rho k_L \vec{u}) = \rho(P_{k_L} - R_{BP} - R_{NAT} - D_L) + \nabla\cdot\left[\mu\nabla k_L\right], \tag{2.9}$$

$$\frac{\partial(\rho\omega)}{\partial t} + \nabla\cdot(\rho\omega \vec{u}) = \rho\left[C_{\omega 1}\frac{\omega}{k_T}P_{k_T} + \left(\frac{C_{\omega R}}{f_W} - 1\right)\frac{\omega}{k_T}(R_{BP} + R_{NAT}) \right. \\ \left. -C_{\omega 2}\omega^2 + C_{\omega 3} f_\omega \alpha_T f_W^2 \frac{\sqrt{k_T}}{d^3}\right] + \\ +\nabla\cdot\left[\left(\mu + \frac{\rho\alpha_T}{\sigma_\omega}\right)\nabla\omega\right]. \tag{2.10}$$

The P-terms express the production of k_T and k_L, D-terms represent the dissipation, and R-terms model the energy transfer from laminar fluctuation to turbulent ones for the so called bypass transition R_{RP} and natural transition R_{NAT} (for details see [21]). We recognized in [22] that the original model fails to correctly capture the position of the natural transition in the case of flows with non-zero pressure gradient. The reason is that the original model detects a critical point for activating R_{NAT} term by using a very simple criterion based on the stability analysis of flows with zero pressure gradient. The original model triggers R_{NAT} when $Re_\Omega = d^2\Omega/\nu$ (here d is the distance to the wall, Ω is the magnitude of vorticity, and ν is the kinematic viscosity) reaches a given constant value. The analysis of the stability for non-zero pressure gradient flows (see e.g. [23]) shows, however, that the loss of stability depends on the pressure gradient. An adverse pressure gradient in decelerating flows typically moves the transition upstream whereas a favorable gradient in accelerating flows delays the transition. Therefore we propose in [22] a modification of the original model which takes into account the pressure gradient.

The natural transition is governed in the original model by the R_{NAT} given as

$$R_{NAT} = C_{R,NAT}\beta_{NAT}k_L\Omega, \tag{2.11}$$

$$\beta_{NAT} = 1 - \exp\left(-\frac{\phi_{NAT}}{A_{NAT}}\right), \tag{2.12}$$

$$\phi_{NAT} = \max\left(Re_\Omega - \frac{C_{NAT,crit}}{f_{NAT,crit}}, 0\right), \tag{2.13}$$

$$f_{NAT,crit} = 1 - \exp\left(-C_{NC}\frac{\sqrt{k_L}d}{\nu}\right). \tag{2.14}$$

The production of laminar kinetic energy k_L is $P_{k_L} = \nu_{T,l}S^2$ with

$$\nu_{T,l} = \min\left\{f_{\tau,l}C_{l1}\frac{\Omega\lambda_{eff}^2}{\nu}\sqrt{k_{T,l}}\lambda_{eff} + \beta_{TS}C_{l2}Re_\Omega d^2\Omega, \frac{k_L + k_{T,l}}{2S}\right\}, \tag{2.15}$$

where

$$Re_\Omega = \frac{d^2\Omega}{\nu}, \tag{2.16}$$

$$\beta_{TS} = 1 - \exp\left(-\frac{\max(Re_\Omega - C_{TS,crit}, 0)^2}{A_{TS}}\right). \tag{2.17}$$

The key role play parameters $C_{TS,crit}$ and $C_{NAT,crit}$. The proposed modification the dimensionless pressure gradient L as

$$\tilde{L} = Re_\Omega^2 \frac{\nu}{U_e^2 ||\vec{U}||} \text{grad} U_e \cdot \vec{U}, \tag{2.18}$$

where $U_e = \sqrt{2(p_{tot} - p)}$ is the estimate of free-stream velocity magnitude. Then the constant values of $C_{TS,crit}$ and $C_{NAT,crit}$ are replaced by

$$C_{TS,crit} = \frac{536.4}{1 - 8.963 \max(\min(\tilde{L}, 0), -1.5)}, \tag{2.19}$$

$$C_{NAT,crit} = \frac{1250}{1 - 8.963 \max(\min(\tilde{L}, 0), -1.5)}. \tag{2.20}$$

The figure 2.1 shows the distribution of pressure and friction coefficient over NACA-0012 profile at $Re = 500\,000$ and angle of attack $\alpha = 0^o$. The original model predicts the transition too late downstream with small separation bubble. On the other hand, the proposed modification captures very well the transition in comparison both with experimental data [24] and with the results obtained with XFoil software [25].

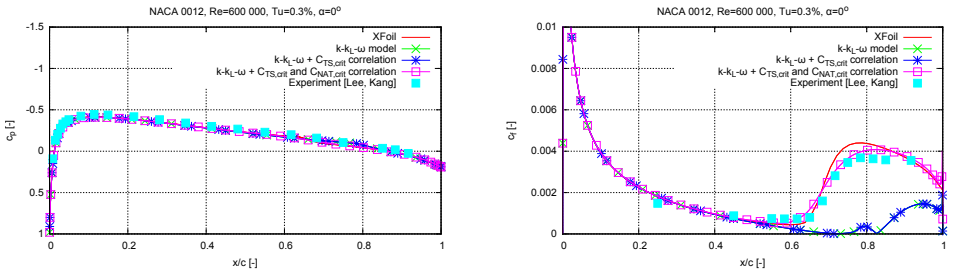

Figure 2.1: Pressure a friction coefficient calculated with and without correlations for $C_{TS,crit}$ and $C_{NAT,crit}$ and comparison with XFoil.

Chapter 3

Numerical methods

The second part of the lecture deals with the numerical solution of the RANS equations (2.1-2.4) with an additional turbulence model. The discretization is achieved with the standard finite volume method in space combined with an explicit or implicit time stepping scheme. The solution is approximated for given time by a piece-wise polynomial function with discontinuities at cell boundaries and the convective fluxes through cell boundaries are evaluated using approximate Riemann solvers (see e.g. [26]). The viscous fluxes are approximated with some variant of central scheme or with a specific variant of the so called diamond cell [27]. It is well known that the basic (first order) scheme with a piece-wise constant approximation of the data is spoiled by a huge amount of numerical viscosity. Therefore, at least a piece-wise linear representation (formally second order scheme) is needed. On the other hand, the stability of the numerical method becomes problematic especially in the case with steep gradients in the solution (shock waves, boundary layers, etc). Therefore some stabilization technique has to be employed. The most widespread one in the finite volume framework is the use of limiters, see e.g. the one-dimensional TVD [28] or NVD [29] limiters, or a multidimensional limiters compatible with modern unstructured finite volume codes [30]. The idea of limiters is to switch to a lower order (and more stable) scheme locally in the vicinity of discontinuities and local extremes. However, with improved stability, this also results in reduced accuracy. Therefore a class of uniformly high order essentially non-oscillatory (**ENO**) schemes has been developed [31]. The ENO schemes were extended for multidimensional case, see e.g. [32], although the implementation (especially the stencil selection) is quite complicated for general unstructured meshes.

3.1 High order WLSQR scheme

In order to simplify the implementation of ENO schemes for unstructured meshes, we proposed in [33] a scheme based on weighted least square interpolation technique. For the sake of simplicity we assume in the following part only a scalar problem without diffusion terms. Although the method is then used for approximation of convective terms for full system of Euler or Navier-Stokes equations.

As a base for our numerical method we use standard finite volume method with data located in centers of polygonal cells. The basic low order semi-discrete method can be written as (see e.g. [34])

$$|\Omega_i|\frac{du_i(t)}{dt} = -\sum_{j\in\mathcal{N}_i} \mathcal{F}(u_i(t), u_j(t), \vec{S}_{ij}). \tag{3.1}$$

Here $u_i(t)$ is the averaged solution over a control volume (or cell) Ω_i, $\mathcal{N}_i$ denotes the set of indices of neighborhoods of Ω_i, $\vec{S}_{ij}$ is the scaled normal vector to the interface between Ω_i and Ω_j (oriented to Ω_j) and $\mathcal{F}$ denotes the so called numerical flux approximating physical flux through the interface between cells Ω_i and Ω_j. A higher order method can be obtained by introducing a cell-wise interpolation $P(\vec{x}; u) = P_i(\vec{x}; u)$ for $\vec{x} \in \Omega_i$ into the basic formula. The higher order method is then formally

$$|\Omega_i|\frac{du_i(t)}{dt} = -\sum_{j\in\mathcal{N}_i} \mathcal{F}(P_i(\vec{x}_{ij}; u), P_j(\vec{x}_{ij}; u), \vec{S}_{ij}), \tag{3.2}$$

where $\vec{x}_{ij}$ is the center of interface between Ω_i and Ω_j. The semi-discrete system is then solved either by an explicit or implicit method. Let us focus the attention to the construction of the piece-wise polynomial approximation P, th so called reconstruction, of the solution from given cell averages. We assume that the reconstruction should satisfy following requirements:

1. **Conservativity**, i.e. the mean value of the interpolant $P(x; u)$ over any cell Ω_i should be equal to cell average of u, in other words

$$\int_{\Omega_i} P(\vec{x}; u)\, d\vec{x} = |\Omega_i| u_i. \tag{3.3}$$

2. **Accuracy**, i.e. for a given smooth function $\tilde{u}(\vec{x})$ with cell averages u_i the interpolant $P(\vec{x}; u)$ should approximate $\tilde{w}$:

$$P(\vec{x}; u) = \tilde{u}(\vec{x}) + \mathcal{O}(h^o), \tag{3.4}$$

   where h is characteristic mesh size and o is the order of accuracy. This accuracy requirement is reformulated in the following way: let us prolongate $P_i(\vec{x}; w)$ over cells in the vicinity of cell Ω_i. Then we request for such cells Ω_j

$$\int_{\Omega_j} P_i(\vec{x}; u)\, d\vec{x} = |\Omega_j| u_j. \tag{3.5}$$

3. **Non-oscillatory**, i.e. the total variation of the interpolant should be bounded for $h \to 0$.

The interpolant $P_i(\vec{x}; u)$ is therefore obtained by minimizing error in (3.5) for Ω_j, $j \in \mathcal{N}_i$ respect to constraint(3.3). In order to mimic weighted ENO method we introduce data dependent weights:

$$P_i(\vec{x}; u) = \arg\min \sum_{j\in\mathcal{N}_i} \left[w_{ij} \left(\int_{\Omega_j} \tilde{P}(\vec{x}; u)\, d\vec{x} - |\Omega_j| u_j \right) \right]^2, \tag{3.6}$$

where minimum is take over over all linear polynomials $\tilde{P}$ satisfying (3.3). We propose in [33] weight

$$w_{ij} = \sqrt{\frac{h^{-r}}{\left|\frac{u_i - u_j}{h}\right|^p + h^q}}, \tag{3.7}$$

with p, q, and r being constants (e.g. $p = 4$, $q = -2$, $r = 3$). The theoretical analysis given in [35] shows that for piece-wise linear reconstruction in 1D the following results hold:

Lemma 3.1.1. *Assume a sufficiently smooth function $u(x)$ having cell averages u_i and weights $w \neq 0$. Then the piecewise linear WLSQR interpolation polynomial approximates $u(x)$ with second order of accuracy, i.e.*

$$P(x; u) = u(x) + \mathcal{O}(h^2). \tag{3.8}$$

In the case of discontinuous data we analyzed the total variation of the interpolant for $u(x)$ defined as $u(x) = 1$ for $x < x_{shock}$ and $u(x) = 0$ for $x \geq x_{shock}$ and we proved for $p = 4$ and q at least in $[-10, 10]$, that the total variation of the interpolant is bounded by

$$TV(P(x; u)) \leq TV(u) + 4h^{1+q/p} + h^{p+q}. \tag{3.9}$$

This yields the following lemma:

Lemma 3.1.2. *Assume weights with*

$$p + q \geq 0, \tag{3.10}$$

$$1 + \frac{q}{p} \geq 0. \tag{3.11}$$

Then the total variation of the interpolant of data given by a single shock with constant states at both sides will be bounded independently of h as $h \to 0$.

In order to asses properties of the method we made several numerical experiments with different weights (see [33]) and finally we chose $p = 4$, $q = -2$, $r = 3$.

The first test deals with the initial value problem for non-linear scalar equation $u_t + uu_x + uu_y = 0$ with periodic initial condition $u_0(x, y) = \sin(2\pi x)\cos(2\pi y)$. The problem was solved with several successive irregular meshes for time $t = 0.1\,\mathrm{s}$ and $t = 0.25\,\mathrm{s}$. The figure 3.1 shows the smooth solution (at the left) and non-smooth solution (at the right).

The figure 3.2 shows the domain, mesh topology, and convergence history for simple test case concerning an inviscid transonic flows through a 2D channel. Numerical experiments have been performed using a structured mesh with 75×25, 150×50, and 300×100 quadrilateral cells and an unstructured mesh with 22 544 triangles. The fluid enters the domain from the left, accelerates over the bump, and leaves the domain to the right. The flow regime corresponds to a transonic flow with inlet Mach number

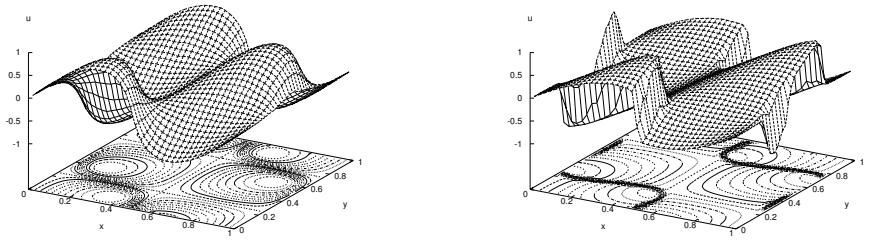

Figure 3.1: Smooth and non-smooth solution of 2D IVP for Burgers equation.

	first order		second order		third order	
$1/N$	$\|\|e\|\|_1$	order	$\|\|e\|\|_1$	order	$\|\|e\|\|_1$	order
	Smooth data ($t = 0.1$)					
0.1	0.054867	-	0.017641	-	0.012703	-
0.05	0.040623	0.43	0.008839	1.00	0.002686	2.24
0.025	0.024009	0.76	0.001963	2.41	0.000648	2.05
0.0125	0.013414	0.84	0.000379	2.37	0.000116	2.48
0.00625	0.007095	0.92	0.000081	2.23	0.000017	2.77
	Non-smooth data ($t = 0.25$)					
0.1	0.112414	-	0.049627	-	0.047704	-
0.05	0.069466	0.69	0.018373	1.43	0.018493	1.36
0.025	0.039077	0.83	0.011098	0.73	0.009987	0.89
0.0125	0.021665	0.85	0.005554	1.00	0.004837	1.05

Table 3.1: Accuracy of the WLSQR scheme for 2D IVP for Burgers equation.

$M_1 \approx 0.675$. The figure 3.2 at the right shows the convergence history for an implicit Euler method. One can see that the low order basic methods converges to steady state faster than higher order methods. Nevertheless both higher order methods using piece-wise linear (denoted by wlsqr2) and piece-wise cubic (wlsqr3) reconstructions converge as well close to machine precision. In general, this is not the case for standard limiters.

The figure 3.3 shows the distribution of Mach number and entropy along the lower side of the channel. One can see that the proposed method provides stable resolution of shock wave without any oscillations. The distribution of entropy shows that the solution obtained with the basic method is heavily spoiled by numerical diffusion. The numerical diffusion is significantly reduced for both reconstructions. The table 3.2 summarizes error analysis using the sequence of three meshes (Π denotes a projection from finer mesh to coarser one). One can see that the parabolic reconstruction slightly reduces the error with respect to linear one but the order of accuracy is not as high as expected due to discontinuity (shock wave) in the date.

Another source of inaccuracy is the polygonal approximation of the domain boundary. In order to improve further the method, we proposed in [36] a scheme for problems with curvilinear boundaries. The boundary is (in 2D)

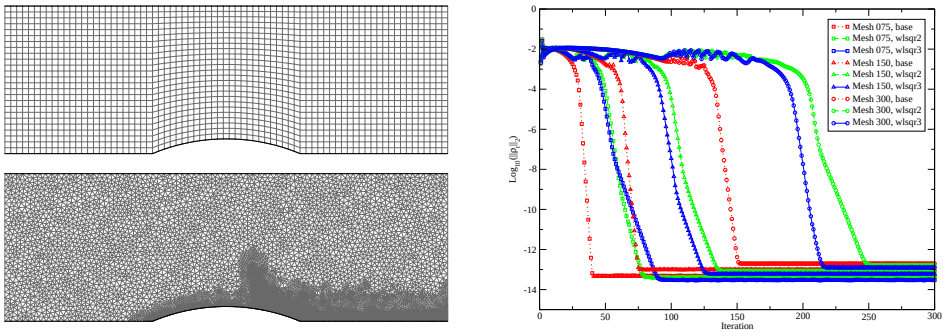

Figure 3.2: Coarse and unstructured meshes and convergence history for 2D test channel.

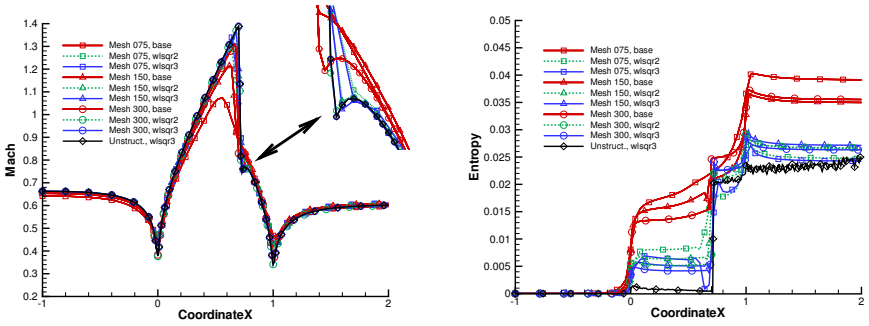

Figure 3.3: Distribution of Mach number and entropy along lower wall of GAMM channel; first order (dotted), second order (dashed) and third order (solid) scheme; coarse (75, rectangles), intermediate (150×50 triangles), fine (300×100, circles), and unstructured (diamonds) mesh.

Reconstruction	$\|\|\rho_h - \Pi^h_{h/2}\rho_{h/2}\|\|_1$	$\|\|\rho_{h/2} - \Pi^{h/2}_{h/4}\rho_{h/4}\|\|_1$	order
None	$6.779 \cdot 10^{-3}$	$3.620 \cdot 10^{-3}$	0.90
Linear	$1.353 \cdot 10^{-3}$	$4.895 \cdot 10^{-4}$	1.46
Parabolic	$1.079 \cdot 10^{-3}$	$4.378 \cdot 10^{-4}$	1.30

Table 3.2: Estimated orders of convergence for GAMM channel benchmark

approximated by piece-wise quadratic curves. The figure 3.4 on the left shows the isolines of Mach number for a so-called Ringleb's flow problem. At the right side of the figure 3.4, the distribution of entropy along the wall obtained with different reconstructions is plotted. The figure summarizes results obtained with linear (I1) and quadratic (I2) reconstruction, and linear (B1) and quadratic (B2) approximation of boundary segments. One can see here quite interesting conclusion that the quadratic scheme combined with linear approximation of boundary (I2B1) gives worse results than linear-linear (i.e. I1B1) scheme. Therefore, the piece-wise quadratic reconstruction has to be combined with at least a pice-wise quadratic approximation of the domain boundary.

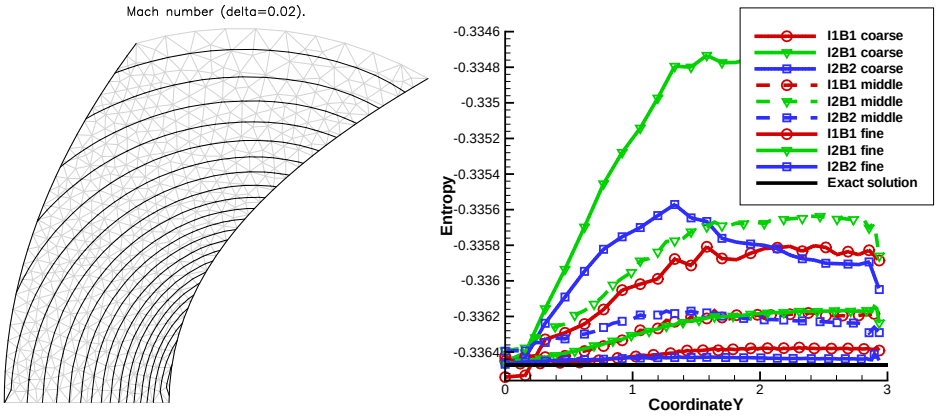

Figure 3.4: Distribution of Mach number for the Ringleb's problem (left) and the distribution of the entropy along the wall (right).

The proposed WLSQR scheme has been extended also for viscous flows using central approximation of viscous fluxes and finally applied to solution of several flow problems including transonic turbulent flows over 2D airfoil profiles, over 3D wings, or through 2D/3D turbine cascades (see e.g. [36]). The figure 3.5 shows the results of simulation of flow through a 2D model of turbine cascade. The calculation of piece-wise quadratic reconstruction was able to capture unsteady effects in the wake, the so called Kármán vortex street.

3.2 An implicit LU-SGS method

Another problem is an efficient solution method for the semi-discrete system (3.1). It is well known that the maximal time-step for the explicit Euler or Runge-Kutta methods is limited by a stability condition. This limitation becomes very strict especially in the case of turbulent flows with high Reynolds numbers where the mesh in the vicinity of the wall has to be very fine (at least in wall normal direction). This makes the use of explicit methods practically useless. Therefore an implicit method or some other acceleration techniques

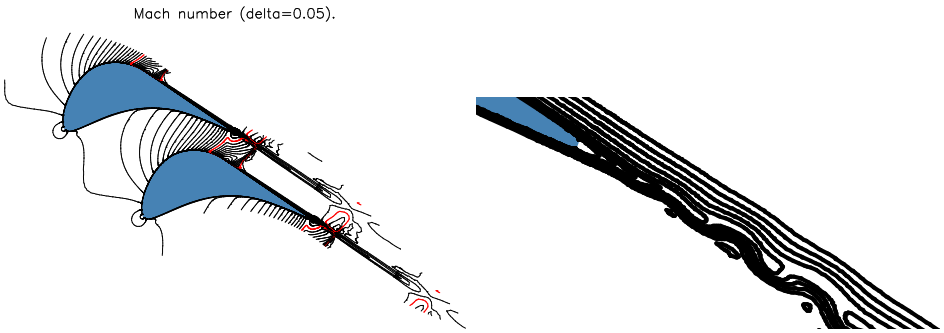

Figure 3.5: Flow through a 2D model of turbine cascade, isolines of the Mach number at the left, details of isolines of entropy at the right.

have to be employed.

We use an implicit method obtained by linearization of the semi-discrete formulation of the finite volume method (3.2). Let's denote $\mathbf{R}^H$ the high order approximation of spatial discretization (the right hand side of (3.2)) and $\mathbf{R}^L$ the low order approximation (the right hand side of (3.1)) written for unknowns $\mathbf{W}$, i.e.

$$\mathbf{R}^H(\mathbf{W})_i = -\sum_{j\in\mathcal{N}_i} \mathcal{F}(P_i(\vec{x}_{ij};\mathbf{W}), P_j(\vec{x}_{ij};\mathbf{W}), \vec{S}_{ij}), \tag{3.12}$$

$$\mathbf{R}^L(\mathbf{W})_i = -\sum_{j\in\mathcal{N}_i} \mathcal{F}(\mathbf{W}_i(t), \mathbf{W}_j(t), \vec{S}_{ij}). \tag{3.13}$$

Then the linearized implicit Euler method can be devised (here $\Delta\mathbf{W}^n = \mathbf{W}_j^{n+1} - \mathbf{W}_j^n$).

$$|\Omega_i|\frac{\Delta\mathbf{W}_i^n}{\Delta t} = -\mathbf{R}^H(\mathbf{W}^{n+1})_i \approx -\mathbf{R}^H(\mathbf{W}^n)_i - \sum_{j\in\mathcal{N}_i\cup\{i\}} \frac{\partial\mathbf{R}^L(\mathbf{W}^n)_i}{\partial\mathbf{W}_j}\Delta\mathbf{W}_j^n, \tag{3.14}$$

and finally

$$\left[\frac{|\Omega_i|}{\Delta t}\mathbb{I} + \frac{\partial\mathbf{R}^L(\mathbf{W}^n)_i}{\partial\mathbf{W}_i}\right]\Delta\mathbf{W}_i^n + \sum_{j\in\mathcal{N}_i}\frac{\partial\mathbf{R}^L(\mathbf{W}^n)_i}{\partial\mathbf{W}_j}\Delta\mathbf{W}_j^n = -\mathbf{R}^H(\mathbf{W}^n)_i. \tag{3.15}$$

The system of linear equations (3.15) has a large non-symmetric sparse matrix and it can be solved e.g. with the GMRES method [37]. This method (i.e. the equation (3.15) combined with GMRES and the incomplete-LU preconditioning) was formerly used e.g. in [36] and extended to unsteady flows with moving boundaries in [38]. Although this method has been successfully used to simulate number of flow problems including transonic turbulent flows in 3D, it turns out that the construction of the matrix and the solution of the system with GMRES method is very demanding both on the computer memory as well as on the CPU. Therefore we develop a simple matrix-free method based on the lower-upper symmetric Gauss-Seidel (**LU-SGS**) iterations, see [39].

Let $\mathcal{L}_i = \{j \in \mathcal{N}_i : j < i\}$ and $\mathcal{U}_i = \{j \in \mathcal{N}_i : j > i\}$. Then the matrix-free LU-SGS method is realized with following two-step procedure

$$D_i \Delta \mathbf{W}_i^{(1)} = -\mathbf{R}^H(\mathbf{W}^n)_i - \frac{1}{2} \sum_{j \in \mathcal{L}_i} \left[\Delta \mathbf{F}_j^{(1)} \cdot \vec{S}_{ij} - \lambda_{ij}^* \Delta \mathbf{W}_j^{(1)} \right], \tag{3.16}$$

$$D_i \Delta \mathbf{W}_i^{n} = D_i \Delta \mathbf{W}_i^{(1)} - \frac{1}{2} \sum_{j \in \mathcal{U}_i} \left[\Delta \mathbf{F}_j \cdot \vec{S}_{ij} - \lambda_{ij}^* \Delta \mathbf{W}_j \right], \tag{3.17}$$

where $\Delta \mathbf{W}^{(1)} = \mathbf{W}^{(1)} - \mathbf{W}^n$, $\Delta \mathbf{F}_j^{(1)} = \mathbf{F}(\mathbf{W}_j^{(1)}) - \mathbf{F}(\mathbf{W}_j^n)$, $\Delta \mathbf{F}_j = \mathbf{F}(\mathbf{W}_j^{n+1}) - \mathbf{F}(\mathbf{W}_j^n)$, and

$$D_i = \frac{|\Omega_i|}{\Delta t} + \frac{1}{2} \sum_{j \in \mathcal{N}_i} \lambda_{ij}^*. \tag{3.18}$$

The λ_{ij}^* is the spectral radius of Jacobians of fluxes, for details see e.g. [39] or [40].

The LU-SGS method was implemented into freely available OpenFOAM package [41]. The figure 3.6 shows the results obtained for the 2D inviscid flow through a channel from the previous chapter (see e.g. figure 3.2). One can see that the method provides better resolution of shock waves in comparison to OpenFOAM solver based on a pressure correction method (SIMPLE scheme). Moreover, the method is in the case of transonic or supersonic flows more efficient in terms of CPU time than the SIMPLE scheme.

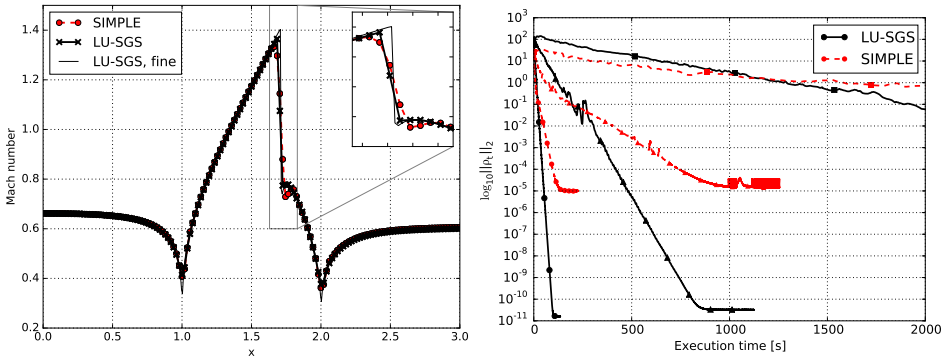

Figure 3.6: Distribution of Mach number lower wall and convergence history (right) for LU-SGS and SIMPLE scheme.

Chapter 4

Applications

In the following section two examples of applications are given. The first one deals with the simulation of 3D flows through an experimental turbine cascade whereas the second one is the flow through a turbine part of a turbocharger.

4.1 Flow through an experimental turbine cascade

The first example deals with a transonic turbulent flow through an experimental turbine cascade TR-L-1 corresponding to mid-section of a rotor blade of last stage of nuclear power plant turbine, see e.g. [42]. The flow through the prismatic cascade was measured at the Institute of Thermomechanics of the Czech Academy of Sciences and the results of the computations were compared to the experimental data. Computations were performed using OpenFOAM package with an in-house LU-SGS solver described in the section 3.2. The flow enters the computational domain with total pressure, total temperature, and inlet direction. The average value of static pressure was prescribed at the outlet. The flow regime is characterized by the Reynolds number $Re = 1.5 \cdot 10^6$ and the isentropic outlet Mach number was $M_{2is} = 1.2$. For other parameters see [42]. The computation has been performed using an unstructured mesh composed of $3.3 \cdot 10^6$ prismatic or hexahedral cells with near wall refinement corresponding to $y^+ \approx 1$. The figure 4.1 shows

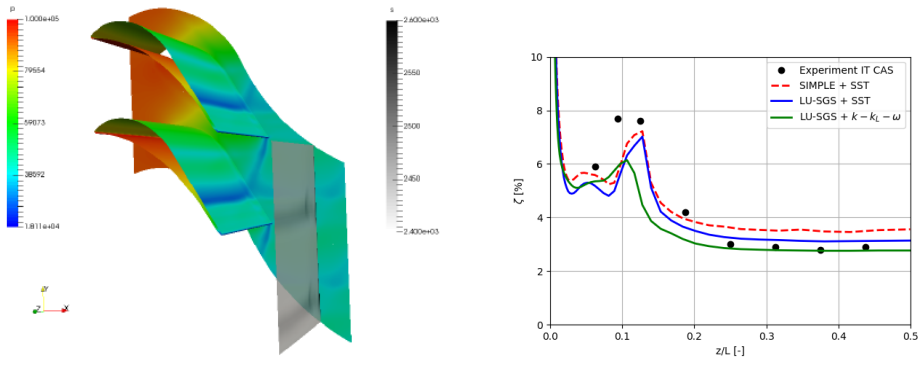

Figure 4.1: Calculated pressure (color) and energy loss coefficient (grayscale) is given at the left, the pitch-wise averaged loss coefficient is given at the right.

the distribution of the pressure at the walls and the energy loss coefficient $\zeta = 1 - \lambda_2^2/\lambda_{2iz}^2$ (here λ is the dimensionless velocity magnitude related to critical sound speed). The figure 4.1 at the right compares the span-wise distribution of the pitch-wise averaged value of energy loss coefficient. One can see that the results obtained with LU-SGS method in combination with the $k - k_L - \omega$ transition and turbulence model agrees very well with the experimental data whereas the pressure correction method based on SIMPLE algorithm in combination with standard SST model overestimates the energy losses. The example show clearly that the choice of a turbulence model and the details of numerical method can have similar impact to the quality of the results.

4.2 Unsteady turbulent flow through a twin-scroll radial turbine

Another application is the simulation of turbulent transonic flow through a radial twin-scroll turbine part of a turbocharger. The figure 4.2 shows the domain containing two inlet tubes, the volute, the rotor of the turbine including the casing, and the outlet tube. The part of computational mesh is shown at the right side of fig. 4.2. The unsteady simulation with time-dependent inlet and outlet boundary conditions extracted from simulation of whole six-piston diesel engine has been performed with the LU-SGS implicit method, see [43].

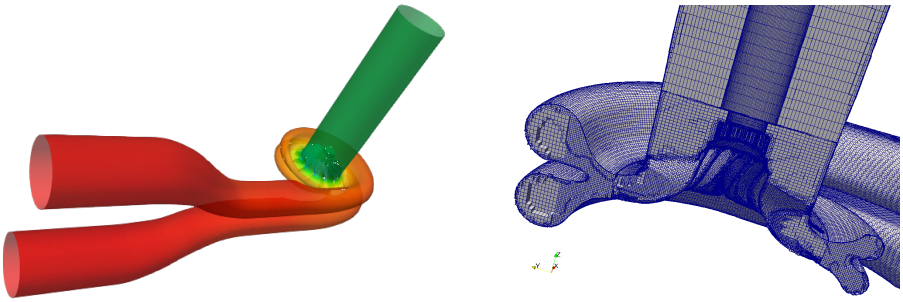

Figure 4.2: Domain and the mesh for twin-scroll turbine simulation

The figure 4.3 (left) shows the comparison of numerically predicted efficiency of the turbine in comparison with results of 1D model calibrated to experimental data [44] and to the measurements for steady state case. One can see quite good agreement of simulation results to experimental data especially at lover blade speed ratios u/c. The right part of figure 4.3 shows the parallel speedup of the solver with respect to one-core (red) or full node (blue) configurations.

The results of transient simulation are displayed at the figure 4.4. The left panel shows the mass flow rate through the turbine outlet in comparison with the results of specifically tuned 1D model. The right panel compares the

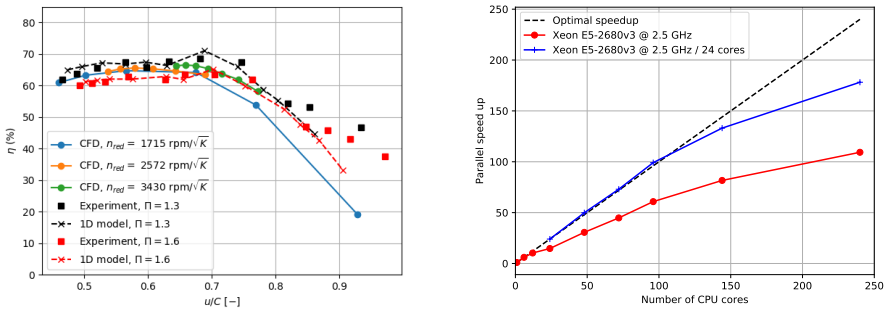

Figure 4.3: The comparison of predictions of turbine efficiency with experimental data (left) and the parallel speedup of the solver (right).

mechanical power produced by the turbine, again compared to 1D model [44]. The predicted average mass flow rate with 3D CFD model $\dot{m} = 0.135\,\mathrm{kg\,s^{-1}}$ differs from the experimental value $0.132\,\mathrm{kg\,s^{-1}}$ by 2.5 %. The 1D model predicts the mass flow rate $0.122\,\mathrm{kg\,s^{-1}}$ which is by 7 % less than the experimental value. The difference between the mass fluxes obtained by 3D CFD and 1D model causes the difference in predictions of average turbine power 11 159 W and 10 180 W, respectively. The main advantage of the 3D CFD method over 1D model is that the full 3D simulation does not need any extra calibration. On the other hand, the 3D method is still very expensive in terms of computational resources.

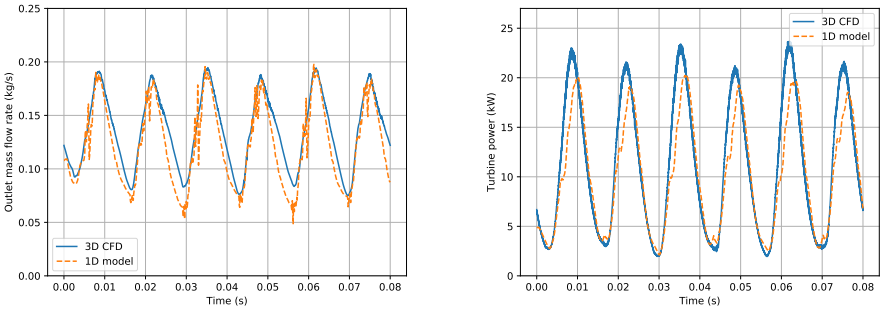

Figure 4.4: Mass flow rate (left) and turbine power (right), comparison of 3D CFD and 1D model for the case of pulsating flow through a turbine

Chapter 5

Outlook of the research and education in the given field

The problem of mathematical modeling and numerical simulation of turbulent flows spreads across several disciplines including numerical mathematics, mechanics of fluids, and computer sciences. Applications are found in many engineering areas including aerospace, turbomachinery, automotive industry, water management, or environmental sciences. Further research in this at the Faculty of Mechanical Engineering will concentrate on:

- development of advanced turbulence models including the hybrid RANS-LES approach,
- development of transition and turbulence models including some effects that have been neglected or overseen so far (e.g. the effects of surface roughness, or improved heat transfer models),
- development of efficient high-order numerical methods for computer simulations of the models of fluids

The research is strongly linked to teaching in master's and doctoral courses it the Faculty of Mechanical Engineering. Moreover, the modeling of turbulent flows provides traditional topics for bachelor, master or doctoral thesis. Student projects range form simple tasks such as e.g. development of 1D models of flows, to more complex one such as development or improvement of turbulence models or development of efficient numerical methods.

Research work carried out by both employees and students is often inspired or directly supported by collaboration with industrial partners such as Doosan Škoda Power a.s., GE Aviation Czech s.r.o., SIGMA Group a.s., or with the univerities as University Paris 13, or Univeristy Toulon.

Bibliography

1. KÁRMÁN, Theodore von. Some Remarks on Mathematics from the Engineer's Viewpoint'. *Mechanical Engineering*. 1940, vol. 62, pp. 308–310.
2. HINZE, J O. *New York*. Turbulence. 2nd. McGraw-Hill College, 1975. ISBN 978-0070290372.
3. CHAPMAN, Gary T.; TOBAK, Murray. Observations, Theoretical Ideas, and Modeling of Turbulent Flows—Past, Present, and Future. In: 1985, pp. 19–49. Available from DOI: 10.1007/978-1-4612-1092-4_2.
4. GUO, Zhaoli; SHU, Chang. *Lattice Boltzmann Method and Its Applications in Engineering*. WORLD SCIENTIFIC, 2013. Advances in Computational Fluid Dynamics. ISBN 978-981-4508-29-2. Available from DOI: 10.1142/8806.
5. GRAHAM, H.W. *Smooth Particle Applied Mechanics: The State Of The Art*. World Scientific Publishing Company, 2006. Advanced Series In Nonlinear Dynamics. ISBN 9789814477185.
6. DEARDORFF, James W. A numerical study of three-dimensional turbulent channel flow at large Reynolds numbers. *Journal of Fluid Mechanics*. 1970. ISSN 14697645. Available from DOI: 10.1017/S0022112070000691.
7. ORSZAG, Steven A.; PATTERSON, G. S. Numerical simulation of turbulence. In: ROSENBLATT, M.; VAN ATTA, C. (eds.). Berlin, Heidelberg: Springer Berlin Heidelberg, 1972, vol. 12, pp. 127–147. Lecture Notes in Physics. ISBN 978-3-540-05716-1. Available from DOI: 10.1007/3-540-05716-1_8.
8. COLEMAN, Gary N.; SANDBERG, Richard D. *A primer on direct numerical simulation of turbulence - methods, procedures and guidelines*. 2010. Technical report. University of Southampton.
9. LAUNDER, B. E.; SPALDING, D. B. *Academic Press*. Lectures in Mathematical Models of Turbulence. 1972. ISBN 0124380506.
10. SMITH, A. M. O.; CEBECI, T. *Numerical solution of the turbulent boundary layer equations*. 1967. Technical report. Douglas aircraft division report DAC 33735.

11. WILCOX, David C. Turbulence and transition modeling for high-speed flows. 1993, vol. 296.

12. MENTER, Florian R. Two-equation eddy-viscosity turbulence models for engineering applications. *AIAA Journal*. 1994, vol. 32, no. 8, pp. 1598–1605. ISSN 0001-1452. Available from DOI: 10.2514/3.12149.

13. HELLSTEN, Antti K. New Advanced k-w Turbulence Model for High-Lift Aerodynamics. *AIAA Journal*. 2005, vol. 43, no. 9, pp. 1857–1869. ISBN 9788578110796. ISSN 0001-1452. Available from DOI: 10.2514/1.13754.

14. MISHRA, Aashwin A.; GIRIMAJI, Sharath S. Toward approximating non-local dynamics in single-point pressure-strain correlation closures. *Journal of Fluid Mechanics*. 2017. ISSN 14697645. Available from DOI: 10.1017/jfm.2016.730.

15. STRELETS, M. Detached eddy simulation of massively separated flows. In: *39th Aerospace Sciences Meeting and Exhibit*. Reston, Virigina: American Institute of Aeronautics and Astronautics, 2001. Available from DOI: 10.2514/6.2001-879.

16. LUO, Da Hai; YAN, Chao; ZHENG, Wei Lin; YUAN, Wu. A New PANS Model for Unsteady Separated Flow Simulations. *Applied Mechanics and Materials*. 2014, vol. 721, pp. 182–186. ISSN 1662-7482. Available from DOI: 10.4028/www.scientific.net/AMM.721.182.

17. SPALART, P. R.; ALLMARAS, S. R. A one-equation turbulence model for aerodynamic flows. In: *30th Aerospace Sciences Meeting and Exhibit*. Reston, Virigina: American Institute of Aeronautics and Astronautics, 1992. Available from DOI: 10.2514/6.1992-439.

18. INGEN, J L Van. Historical review of work at TU Delft. In: *38th Fluid Dynamics Conference and Exhibit*. Seattle, 2008, pp. 1–49. No. June.

19. STRAKA, Petr; PŘÍHODA, Jaromír. Application of the algebraic bypass-transition model for internal and external flows. In: *Experimental Fluid Mechanics 2010*. Liberec, 2010, pp. 636–646.

20. MENTER, Florian R.; LANGTRY, Robin Blair; VÖLKER, S.; HUANG, P. G. Transition Modelling for General Purpose CFD Codes. *Engineering Turbulence Modelling and Experiments 6*. 2005, no. August, pp. 31–48. ISBN 9780080445441. ISSN 1386-6184. Available from DOI: 10.1016/B978-008044544-1/50003-0.

21. WALTERS, D. Keith; COKLJAT, Davor. A three-equation eddy-viscosity model for Reynolds-averaged Navier–Stokes simulations of transitional flow. *Journal of Fluids Engineering*. 2008, vol. 130, no. 12, pp. 121401–121401–14. ISBN 0098-2202. ISSN 00982202. Available from DOI: 10.1115/1.2979230.

22. FÜRST, Jiří; ISLAM, Mazharul; PŘÍHODA, Jaromír; WOOD, David. Towards pressure gradient sensitive transitional k-kL-omega model: The natural transition for low Re airfoils. In: IT CAS v.v.i., 2015, pp. 65–70. ISSN 2336-5781.

23. SCHLICHTING, H.; ULRICH, A. Zur Berechnung des Umschlages laminar-turbulent. *Luftfahrtforschung*. 1942, vol. 1, pp. 8–35.

24. LEE, H.; KANG, S. Flow characteristics of transitional boundary layers on an airfoil in wake. *Journal of Fluids Engineering*. 2000, vol. 122, pp. 522–532.

25. DRELA, Mark. XFOIL: An analysis and design system for low Reynolds number airfoils. In: MUELLER, T. J. (ed.). *Low Reynolds Number Aerodynamics*. 1989, vol. 54, pp. 1–12. Lecture Notes in Engineering. Available from DOI: 10.1007/978-3-642-84010-4_1.

26. TORO, Eleuterio F. *Riemann Solvers and Numerical Methods for Fluid Dynamics*. Berlin, Heidelberg: Springer Berlin Heidelberg, 2009. ISBN 978-3-540-25202-3. Available from DOI: 10.1007/b79761.

27. COIRIER, William; POWELL, Kenneth. A Cartesian, cell-based approach for adaptively-refined solutions of the Euler and Navier-Stokes equations. In: *33rd Aerospace Sciences Meeting and Exhibit*. Reston, Virigina: American Institute of Aeronautics and Astronautics, 1995. Available from DOI: 10.2514/6.1995-566.

28. HARTEN, Ami. High Resolution Schemes for Hyperbolic Conservation Laws. *Journal of Computational Physics*. 1997, vol. 135, no. 2, pp. 260–278. ISSN 00219991. Available from DOI: 10.1006/jcph.1997.5713.

29. LEONARD, B.P. A stable and accurate convective modelling procedure based on quadratic upstream interpolation. *Computer Methods in Applied Mechanics and Engineering*. 1979, vol. 19, no. 1, pp. 59–98. ISSN 00457825. Available from DOI: 10.1016/0045-7825(79)90034-3.

30. BARTH, Timothy; JESPERSEN, Dennis. The design and application of upwind schemes on unstructured meshes. In: *27th Aerospace Sciences Meeting*. Reston, Virigina: American Institute of Aeronautics and Astronautics, 1989. Available from DOI: 10.2514/6.1989-366.

31. HARTEN, Ami; ENGQUIST, Bjorn; OSHER, Stanley; CHAKRAVARTHY, Sukumar R. Uniformly high order accurate essentially non-oscillatory schemes, III. *Journal of Computational Physics*. 1987, vol. 71, no. 2, pp. 231–303. ISSN 00219991. Available from DOI: 10.1016/0021-9991(87)90031-3.

32. ABGRALL, R. On Essentially Non-oscillatory Schemes on Unstructured Meshes: Analysis and Implementation. *Journal of Computational Physics*. 1994, vol. 114, no. 1, pp. 45–58. ISSN 00219991. Available from DOI: 10.1006/jcph.1994.1148.

33. FÜRST, Jiří. A weighted least square scheme for compressible flows. *Flow, Turbulence and Combustion*. 2006, vol. 76, no. 4, pp. 331–342. ISBN 1049400690. ISSN 1386-6184. Available from DOI: 10.1007/s10494-006-9021-y.

34. FEISTAUER, Miloslav; FELCMAN, Jiří; STRAŠKRABA, Ivan. *Mathematical and computational methods for compressible flow*. Clarendon Press, 2003. ISBN 0198505884.

35. FÜRST, Jiří. Numerical Solution of Inviscid and Viscous Flows Using Weighted Least Square Scheme and Quadrilateral or Triangular Mesh. In: *Czech-Japanese Seminar in Applied Mathematics*. 2004, p. 8.

36. FÜRST, Jiří. The high order WLSQR scheme and its applications in turbomachinery. In: *Computational Fluid Dynamics 2006 - Proceedings of the Fourth International Conference on Computational Fluid Dynamics, ICCFD 2006*. springer berlin, 2009, pp. 155–160. Available from DOI: 10.1007/978-3-540-92779-2-22.

37. SAAD, Youcef; SCHULTZ, Martin H. GMRES: A Generalized Minimal Residual Algorithm for Solving Nonsymmetric Linear Systems. *SIAM Journal on Scientific and Statistical Computing*. 1986, vol. 7, no. 3, pp. 856–869. ISSN 0196-5204. Available from DOI: 10.1137/0907058.

38. FÜRST, Jiří. The Implicit WLSQR Scheme for Unsteady Flows. In: *Topical Problem of Fluid Mechanics*. Institute of Thermomechanics AS CR v.v.i., 2006, pp. 59–62.

39. FÜRST, Jiří. Development of a coupled matrix-free LU-SGS solver for turbulent compressible flows. *Computers & Fluids*. 2018, vol. 172, pp. 332–339. ISSN 00457930. Available from DOI: 10.1016/j.compfluid.2018.04.020.

40. BLAZEK, Jiri. *Computational fluid dynamics : principles and applications*. Butterworth-Heinemann, 2015. ISBN 9780128011720.

41. WELLER, H. G.; TABOR, G.; JASAK, H.; FUREBY, C. A tensorial approach to computational continuum mechanics using object-oriented techniques. *Computers in Physics*. 1998, vol. 12, no. 6, pp. 620. ISSN 08941866. Available from DOI: 10.1063/1.168744.

42. ŠIMURDA, David; FÜRST, Jiří; LUXA, Martin. 3D flow past transonic turbine cascade SE 1050 - Experiment and numerical simulations. *Journal of Thermal Science*. 2013, vol. 22, no. 4, pp. 311–319. ISSN 10032169. Available from DOI: 10.1007/s11630-013-0629-7.

43. FÜRST, Jiří; ŽÁK, Zdeněk. Numerical simulation of unsteady flows through a radial turbine. *Advances in Computational Mathematics*. 2019. ISSN 1019-7168. Available from DOI: 10.1007/s10444-019-09670-4.

44. MACEK, Jan; ŽÁK, Zdeněk; VÍTEK, Oldřich. Physical Model of a Twin-scroll Turbine with Unsteady Flow. In: *SAE 2015 World Congress & Exhibition*. SAE International, 2015, p. 14. Available from DOI: 10.4271/2015-01-1718.